A study of the tracking performance of irradiated SCT prototypes using test beam data.

M.Vos [a,b], M.D'Onofrio [c], J.E.Garcia Navarro [a], G.F.Moorhead [d]

[a] *IFIC, U. Valencia/CSIC, Spain*
[b] *Universiteit Twente, The Netherlands*
[c] *University of Geneva, Switzerland*
[d] *University of Melbourne, Australia*

Abstract

In beam tests of SCT module prototypes, tracking efficiency and noise occupancy per detector plane are routinely measured. ATLAS simulations, on the other hand, predict the efficiency and fake rates for the complete inner detector in a realistic environment. In the H8 test beam in August 2002 an attempt was made to bridge the gap between simulation and measurement. To this end tracks were reconstructed using only the information from an array of prototype SCT modules. In this note the most important results are presented.

1 Introduction

Due to the high multiplicity of charged tracks the ATLAS inner detector is a challenging environment for pattern recognition and tracking algorithms. During high luminosity operation the occupancy due to real tracks, from the trigger event plus a number of pile up events (underlying minimum bias events), is expected to be as high as 0.6 % [1] in certain regions of the SCT.

Detailed simulations have been performed and were reported in the inner detector Technical Design Report [1]. The pattern recognition is expected to be quite robust as long as the noise occupancy is maintained below a tolerable level. Radiation damage of the detector during operation is expected to lead to a noise increase and a deterioration of the collected charge. In the SCT design the noise occupancy and single plane efficiency are specified to be $5 \cdot 10^{-4}$ and 99 %.

2 March 2003

Beam tests have been performed on many prototype modules in recent years, see references [2–8] and the barrel and forward module Final Design Reports. The single track, single detector plane tracking efficiency is found to be over 99%, while the noise occupancy is well below the specificied level. Modules irradiated to twice the expected maximum fluence ,$3 \cdot 10^{14}$ 24 GeV p/cm^2, are observed to have a narrow operating margin (the operating margin is the range of discriminator thresholds where both the efficiency and noise occupancy specifications are met).

In the August 2002 beam test in the H8 beam line in the CERN SPS four irradiated barrel module prototypes and three irradiated prototypes of end-cap geometry were read out simultaneously. These data provide an opportunity to cross-check the claim that high tracking performance can be achieved on a complex multi-module system, even after the charge collection and noise performance have deteriorated due to radiation damage. In this note the results of a tracking study on these irradiated prototype modules are reported.

The first section, 2, briefly introduces the H8 setup and the modules under study. In the analysis section, 3, the definitions of efficient, and fake tracks in the beam test environment are discussed. Results of an analysis of the data from a four-module barrel and a three-module end-cap array are reported in section 4. In section 5 the tracks are fitted to a helix. The results are compared to a simulation of the stand-alone SCT. Extrapolation of the results to the performance of the inner detector is not straight-forward. Therefore, in section 6 some of the differences between ATLAS and test beam tracking study are discussed together with possible ways to improve the test beam analysis. The final section, 7, summarizes the findings.

2   Setup

The SCT test beam setup in H8 has been described extensively elsewhere [3–8]. This section is therefore limited to a brief description of the modules under test and a few points that are of specific interest to the tracking study.

Figure 1 shows the arrangement of the modules in the H8 beam line. The modules are held in a light-tight thermally insulating box encompassed by the beam telescope.

Four irradiated barrel modules - 0044, 0047, 007 and 0034 - make up the barrel tracking array. A second array consists of three irradiated end-cap modules: K5-310, K5-312 and K5-308. The separations between the modules were chosen to coincide as well as possible in the test beam mechanics with the distance between consecutive SCT barrels ($d = 90$ mm in H8 versus $\Delta R = 73$ mm in
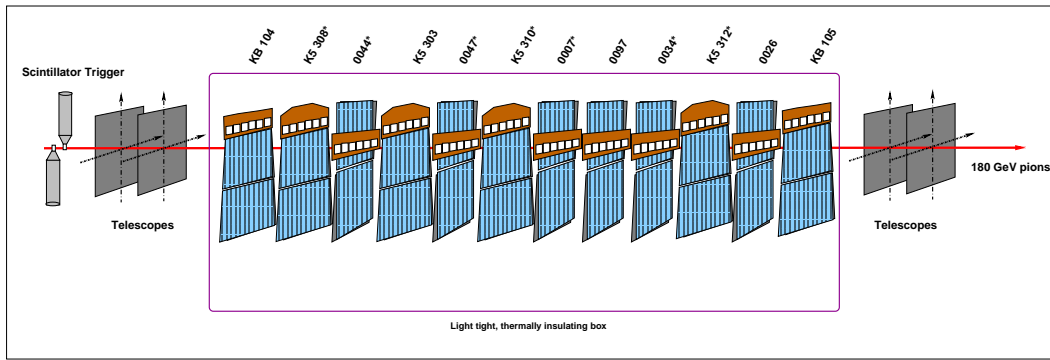
Fig. 1. Arrangement of the SCT prototype modules in the beam line during the tracking study.

ATLAS) and wheels ($d = 180$ mm in H8 versus $\Delta z_{3-4} = 188$ mm , $\Delta z_{4-5} = 188$ mm in ATLAS).

In the electrical readout scheme employed in H8, the timing of the modules cannot be fine-tuned. To reduce the sensitivity to the timing of individual modules the logical OR of the hit pattern from the three time bins is taken as the binary result (ANYHIT or XXX data compression, see [9]). The noise occupancy in this mode is nearly a factor three higher than in LEVEL (X1X) or EDGE (01X) compression. Therefore, ATLAS and standard test beam analysis use more aggressive compression modes. The discriminator is set to edge sensing mode throughout the tracking study as this is the envisaged operating mode for ATLAS.

All modules in the tracking study, marked with an asterisk (*), had been irradiated in the CERN PS to a target fluence of $3 \cdot 10^{14}$ protons/cm^2. Exact fluences are currently subject to investigation. Figure 2 shows the single-module efficiency and noise occupancy for the modules involved. The barrel modules have a rather uniform behaviour. One of the end-cap modules, however, has a significantly higher noise and less charge margin than the other two. In the compression mode used here, a threshold of 1.2 ±0.1 fC is required to reach the specified noise occupancy of $5 \cdot 10^{-4}$ on all modules.

The telescope system is able to reconstruct and interpolate tracks with a precision of a few microns. The internal alignment of the telescope-DUT system is found using an iterative algorithm that minimizes the residuals of the tracks, see reference [3] for a more detailed description. The error associated with the alignment is small compared to the reconstruction precision of a single track. The VA2 readout chips of the telescope modules have a rather long peaking time ($1\mu s$). Therefore, occasionally multiple tracks are found. The geometrical acceptance of the telescope is 3.2 × 3.2 cm, significantly smaller than the DUTs, but large compared to the size of the beam spot of 0.5 × 1.0 cm.

The operating parameters under study here are the discriminator threshold
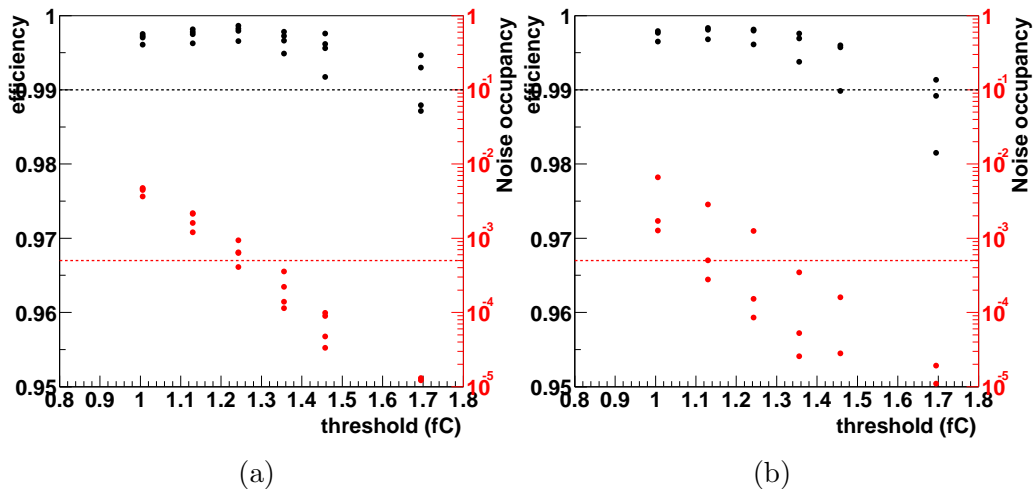
3

Fig. 2. Module efficiency and noise occupancy versus discriminator threshold for the four barrel modules in this study *(a)* and the three end-cap modules *(b)*. Note that these results are for ANYHIT compression, edge sensing ON and can differ substantially from the standard results in [2].

setting and the detector bias voltage. After characterization of the Front End response the threshold is conveniently expressed in terms of equivalent input charge (fC). The threshold values shown on the plot axes are corrected by a global factor 1.13 to account for the deviation from the nominal value of the calibration capacitor [1]. The detector bias voltage is a function of the supply voltage and the leakage current at that voltage [2]. The leakage current of the irradiated modules varied between 1 and 3 mA, leading to an on-detector voltage of 470 to 490 Volts.

The basic unit of data is a run of 25000 events. Runs were taken at different thresholds around the envisaged 1 fC operating point: 0.7, 0.9, 1.0, 1.1, 1.2, 1.3, 1.5, 2.0 fC to evaluate the effect of the discriminator threshold and thus the occupancy on the tracking performance. This basic scan was repeated for two detector bias voltages: 500 and 400 Volts. For two strategic thresholds - the nominal 1 fC and the threshold where the noise occupancy is below the specified $5 \cdot 10^{-4}$, 1.2 fC - a detailed scan of detector bias voltage was performed, consisting of: 350, 375, 400, 425, 450, 475 and 500 Volts.

---

[1] Individual correction factors are known for these modules, but were not applied online.

[2] The 11 $k\Omega$ resistor in the HV filter on the hybrid causes a voltage drop proportional on the leakage current

3 Analysis

The first step in the analysis is selection of the events that will be analysed. With these events, a track finder builds a sample of candidate tracks. On the basis of a track quality parameter it is decided to keep or discard a candidate. The accepted tracks are evaluated, comparing with the track reconstructed using the beam telescope. In this section, the analysis is described. Efficiency and fake and spoiled tracks are defined here. Finally, some example events are shown to clarify these definitions.

Event selection. After each scintillator trigger the three subsystems, binary modules, beam telescope and the TDC measuring the trigger phase with respect to the system clock, are read out. Only events that satisfy the following criteria are accepted in the analysis:

- exactly one reconstructed track in the telescope
- the track is required to be straight and parallel to the beam axis within certain tolerances
- at least one plane of the anchor module is required to be efficient
- no more than 8 hits in the analog telescope

The first three criteria are standard test beam procedure. The first cut eliminates those events where the track fell outside the telescope acceptance or a second track was found. The second cut is designed to eliminate tracks that suffered multiple scattering during its path through the setup. The third requirement eliminates events where the data was corrupted, synchronicity between subdetectors was lost, etc. The fourth cut is specific to this study. It was introduced to reduce the effect of hard interactions producing a second charged track in the setup. These are of course rather rare, but can create "fake" tracks at rates comparable to the ones measured.

Track finder. For the remaining events, a track finder algorithm reconstructs candidate tracks using only the binary information from the SCT modules.

The first step combines the hits on both sides of each module into space points with associated errors. The intersection of two 80 micron wide strips defines a rhomb with short axis $\frac{p}{\cos\alpha/2}$ and long axis $\frac{p}{\sin\alpha/2}$, where p is the readout pitch and α is the stereo angle. The short axis corresponds with the X axis of our global coordenate system, while the long axis is identified with the Y axis. Projecting the uniform distribution in the rhomb on both axes yields triangular distributions with an RMS of ~ 17 microns in X and ~ 810 microns in Y, see figure 3. More detailed single module resolution were reported in reference [3]. All valid space points, ie those that fall within the active area of the module, are stored in a list.
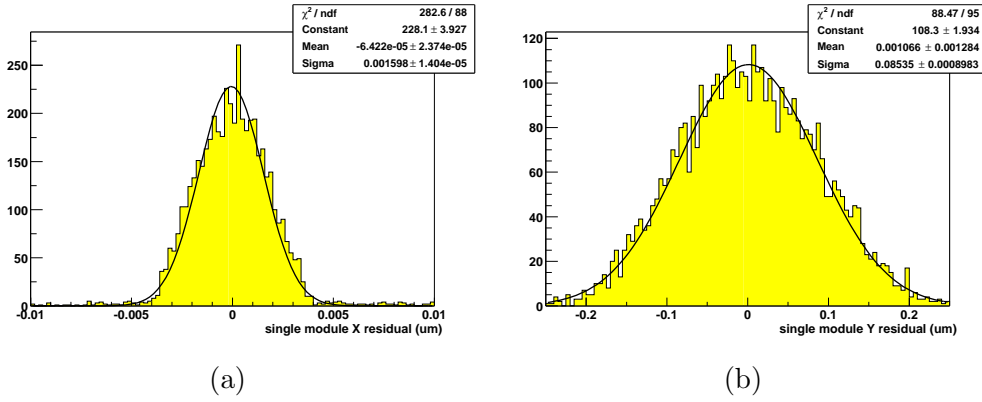
χ^2 / ndf	282.6 / 88
Constant	228.1 $\pm$ 3.927
Mean	-6.422e-05 $\pm$ 2.374e-05
Sigma	0.001598 $\pm$ 1.404e-05

χ^2 / ndf	88.47 / 95
Constant	108.3 $\pm$ 1.934
Mean	0.001066 $\pm$ 0.001284
Sigma	0.08535 $\pm$ 0.0008983

(a)   (b)

Fig. 3. Residuals of the space point reconstructed on a single (barrel) module wrt the position interpolated from the beam telescope measurements: *(a)* X position *(b)* Y position

The track finder creates track stubs between all possible pairs of XY points on different modules. For each stub the relevant region on the remaining modules is searched for the XY points closest to the track. If the required number of space points is found, the stub becomes a track candidate. A candidate track is accepted if the χ^2 of the track fit is smaller than a certain value.

Track analysis.

The error on the X and Y intercept depends on the number of points and the error on each point. It further depends on the separation between the measurements and the z position where the intersect is evaluated. For a straight line fit through N points with error σ_i and:

$$\sigma^2(intersect) = \frac{\sigma_i^2}{N}[1 + \frac{\sigma_{x,y}^2(z_0 - <z>)^2}{N(<z^2> - <z>^2)}]$$

The second term vanishes when the z position is chosen to be the center of the tracker ($z = <z>$).

Comparison between the intersects of the tracks reconstructed using the information of the binary tracking array and of the analog beam telescope yield the residual distributions of figures 4(a) and 4(b). The width of the Y intersect residual is close to the expect 405 microns. The X residual is slightly broader than the expected 8-9 microns due to the - no longer negligible - error in the interpolation of the beam telescope track.

Whereas the position distributions are close to Gaussian, the residual distributions of the track slopes of figures 4(c) and 4(d) show distinctive multi-peak-features due to the discrete nature of the measurements of strip detectors with binary readout. The exact shape of the multi-peak distributions depends on

6

the relative alignment of the detector planes, which is not controlled in the test beam. These effects have been discussed in the context of the alignment of the SCT [10] and have been observed in previous beam tests [4]. The errors σ_i are taken to be the RMS of the distributions of figure 4(a) to 4(d).
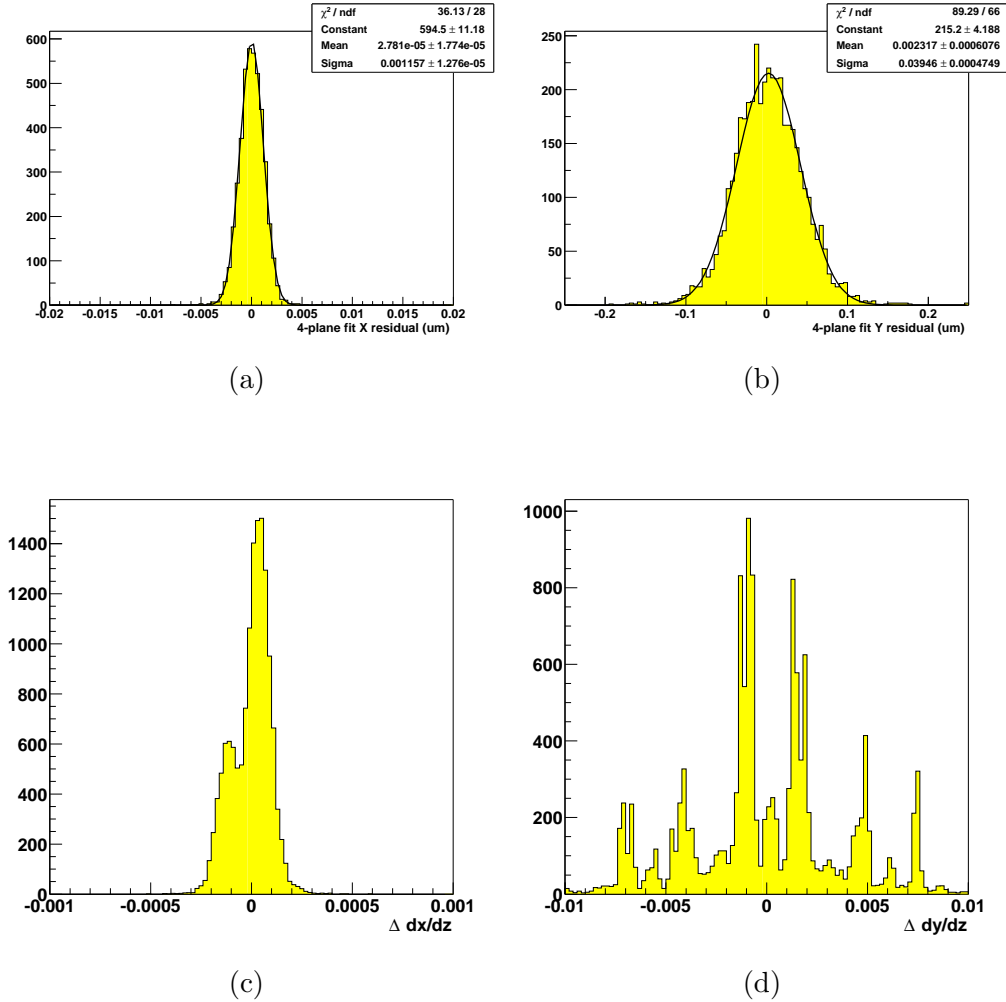

(a)

(b)

(c)

(d)

Fig. 4. Difference in track parameters between the track reconstructed from the beam telescope information and from a four-barrel-module array: *(a)* X position *(b)* Y position *(c)* X slope wrt beam axis *(d)* Y slope wrt beam axis

To evaluate whether the reconstructed track corresponds to a real particle or is a "fake" its parameters are compared to those of the beam telescope track. The distance between the two tracks is defined as the difference of the track parameters weighed by their errors:

$$d_{track} = \sum \frac{|a_i^{tel} - a_i^{bin}|}{\sigma_i} \tag{1}$$

7

,where the a_i are the track parameters and the σ_i their errors. A track is considered "good" if its distance to the telescope track d_{track} is smaller than 20 sigma. An event is labeled efficient if at least one "good" track is found. The remaining tracks are labeled as fakes. This definition of fake includes "spoiled" tracks, ie tracks where the track parameters are badly distorted due to incorrect hits.

Examples. The displays of figure 5 to 8 show a number of typical events. All figures show an XZ and YZ view, where Z is the beam axis. The leftmost and rightmost rectangles represent the XY positions of combinations of hits in the X and Y plane of the upstream and downstream telescope modules. XY points on SCT modules are drawn as rectangles, where the size indicates the one sigma error on the position. The track or tracks reconstructed through the SCT points is shown as a straight line. Combinations of signal hits with noise hits lead to extra XY points that do not coincide with the track.

Figure 5 shows how a single track is detected by the telescope modules and the SCT modules. No incorrect hits are found close to the track and the reconstruction is unambiguous. Figures 6 shows an event taken at a lower
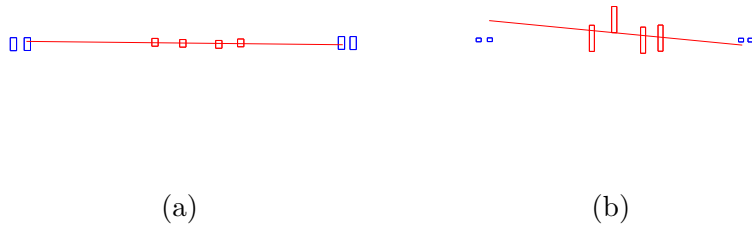

(a)   (b)

Fig. 5. Example of a perfectly normal event: *(a)* XZ view *(b)* YZ view

discriminator threshold. The track finder now has to find the track from among a large number of incorrect XY points. Apart from the real track a fake track is reconstructed through three incorrect and one correct hit.

Figures 7 and 8 show two examples of problematic events, where an apparent fake track is created by real particles. Figure 7 shows a rare event, where an interaction occurs within the volume of the tracker. The collision of the beam pion knocks an electron out of its atom, creating a second (real) track. Whenever the outgoing tracks fall in the telescope acceptance these events can be identified by the extra hits in the telescope and discarded from the analysis.

Figure 8 shows an event where two parallel tracks enter the tracking volume. The telescope only reconstructs one of them as the second track falls outside
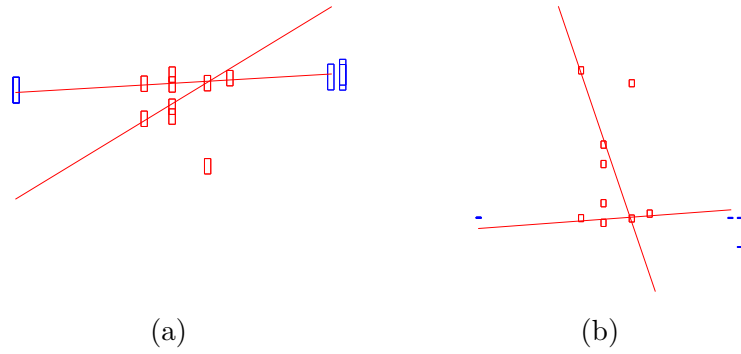
(a)   (b)

Fig. 6. Example of a typical fake track: *(a)* XZ view *(b)* YZ view

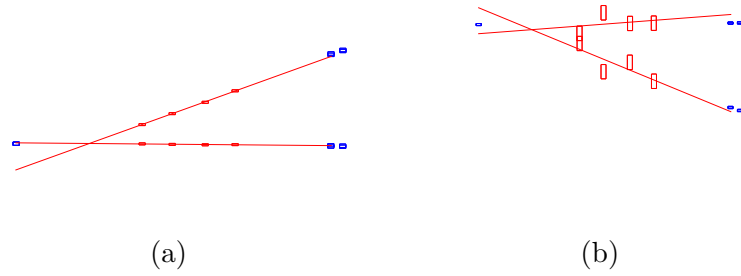(a)   (b)

Fig. 7. Example of an event where a second track is due to a hard interaction in the tracking volume: *(a)* XZ view *(b)* YZ view

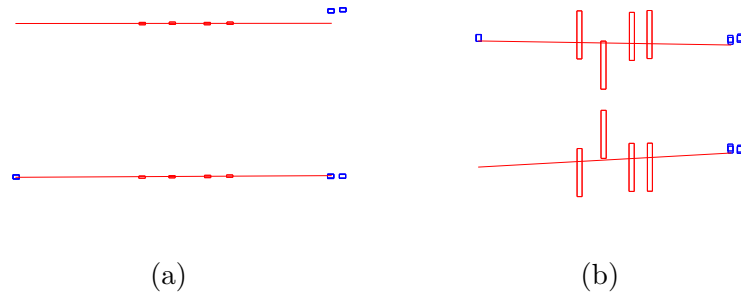(a)   (b)

Fig. 8. Example of an event where two real tracks enter the tracking volume: *(a)* XZ view *(b)* YZ view

the telescope acceptance on the $z = 0$ end. Again, only two-tracks events that fall in the acceptance of the telescope can be identified. Events like the ones in figures 7 and 8 contribute to the measured fake rate. After cuts on the telescope multiplicity the contribution is approximately $10^{-5} - 10^{-4}$, of the same order as the statistical error.

9

4 Results

The measurement of the tracking efficiency and the fake rate of course depends on the choice of the track quality cut. A loose cut reduces the loss of efficiency, but will also lead to an unnecessarily high fake rate. Figures 9 show the effect of the χ^2 cut applied in the analysis. For three cases, a three module end-cap tracking array and a three and four module barrel tracker, the tracking efficiency and fake rate corresponding to a threshold of ~ 1.2 fC and a supply bias voltage of 500 Volts are shown.

In the three tracking setups the efficiency rises steeply as the χ^2 cut is loosened and more tracks are accepted. The optimum value for the cut is a compromise between efficiency and fake rate. For the remainder of this analysis the χ^2 cut is set to 5.

The steps in the fake rate in the top figure in 9 are due to the limited statistics. In the bottom figure in 4 the fake rate vanishes compared to the measurement error. For fake rates of the order of 10^{-4}, 95% confidence level upper limits are calculated. Lower limits are not calculated as at this level the rate is dominated by real tracks as in figures 7 and 8 in section 3.

Figures 10 present the tracking efficiency and fake rate result for the optimised cut values. The top and central figures in 10 correspond to the three-module end-cap and barrel arrays respectively. In both cases the maximum efficiency is over 97 %, obtained at a threshold of ~ 1.2 fC.

The fake rate is a steep function of threshold (occupancy) in both three-module arrays. At the threshold where the noise occupancy is around $5 \cdot 10^{-4}$ - ~ 1.2 fC - the fake rate has dropped to a few times 10^{-3}. A further increase of the threshold does not lead to a significant reduction of the fake rate. The fake rate is lower in the end-cap array, as a result of the low occupancy of 310 and 312. The probability to reconstruct fake tracks is highest when the noise occupancy is distributed evenly among the modules, like in the barrel array.

From a comparison of the central and bottom figures in 10 it is clear that the addition of a fourth XY point very efficiently reduces the fake rate, while the tracking efficiency is virtually unaffected. From a threshold of 1.2 fC upward the fake rate is compatible with 0.

The results of figure 10 correspond to a relatively high detector bias voltage of 470-490 Volts. Running at a lower voltage leads to a loss of charge collection efficiency due to increased trapping of the carriers in radiation induced lattice defects. If the collected charge deteriorates too much the efficiency will be affected. Figures 11 show the tracking efficiency dependence on the supply bias voltage for a fixed threshold of 1.2 fC.
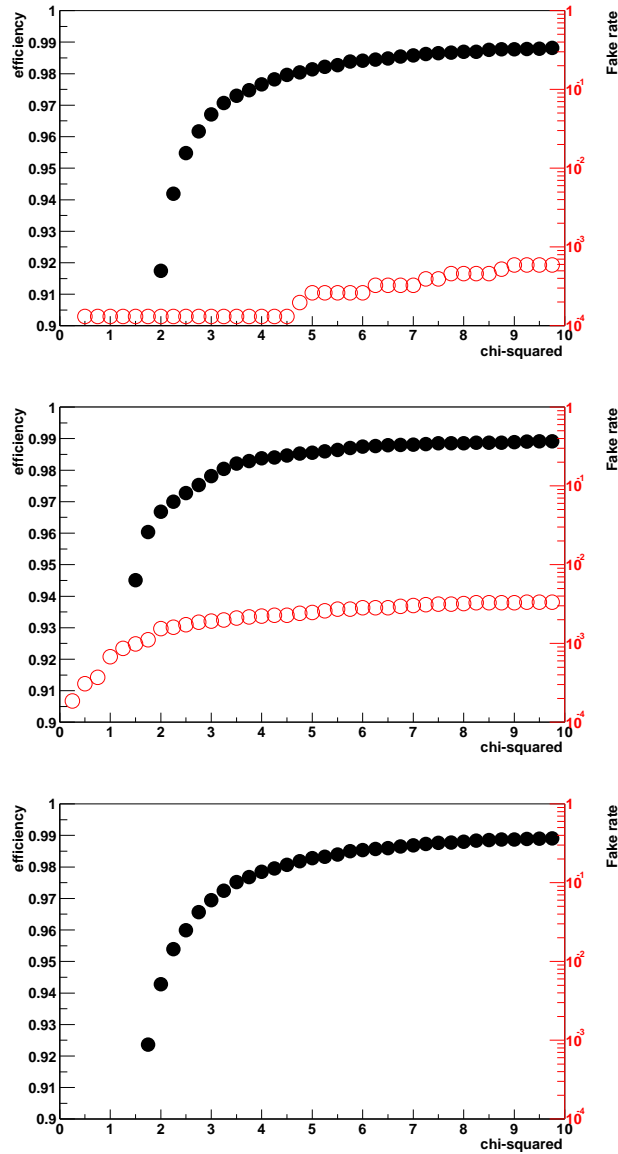
Fig. 9. Tracking efficiency (filled markers) and fake rate (open markers) versus the track quality cut. The discriminator threshold is set to a nominal threshold of 1.1 fC on all modules, corresponding to ~ 1.2 fC after correction of the calibration capacitor. Detector bias is 500 Volts on the HV supply, resulting in 470-490 Volts on the detector. A tracking array consisting of three end-cap modules: 312, 310 and 308*top*, three barrel modules: 0034, 007 and 0047 *center* and a four module barrel array, the three previous plus 0044 *bottom*.

In the three tracking arrays around 1-2 % of efficiency is lost when the detector bias is lowered to 370-390 Volts. No significant dependence of the fake on bias voltage is observed.

The behaviour of the tracking efficiency as a function of discriminator threshold and bias voltage is close to what one would expect. As a hypothesis we
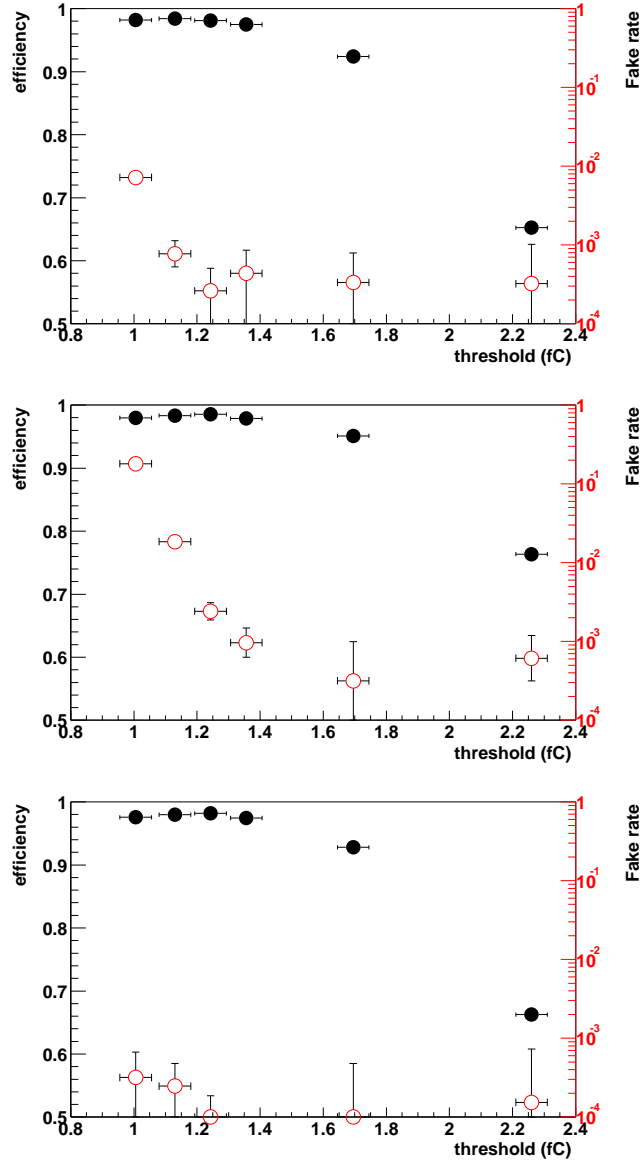
11

Fig. 10. Tracking efficiency and fake rate versus (corrected) discriminator threshold. Detector bias is 500 Volts on the HV supply, resulting in 470-490 Volts on the detector. A tracking array consisting of three end-cap modules: 312, 310 and 308 *(top)*, three barrel modules: 0034, 007 and 0047 *(center)* and a four module barrel array, the three previous plus 0044 *(bottom)*.

postulate that the tracking efficiency is the product of the efficiencies of the individual planes that make up the tracker:

$$\epsilon_{tracking} = \prod_{i=1}^{n} \epsilon_i \qquad (2)$$

,where n is the number of detector planes, ie twice the number of modules, in the tracker and the ϵ_i are the plane efficiencies.
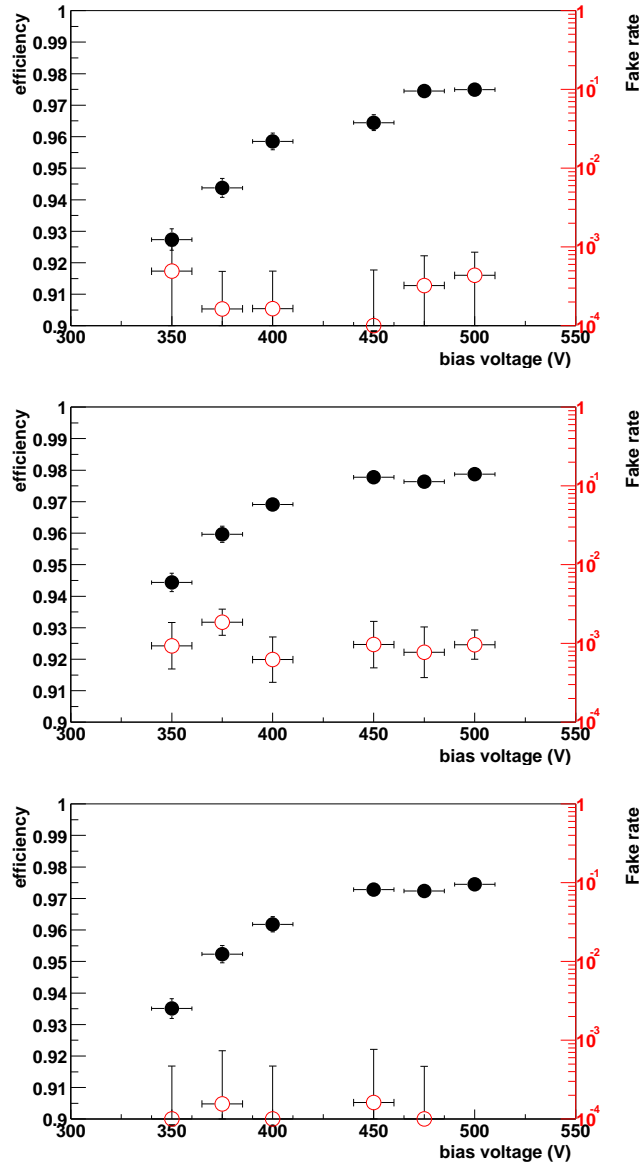
Fig. 11. Tracking efficiency and fake rate versus supply bias voltage. The discriminator threshold is set so that the average noise occupancy is below $5 \cdot 10^{-4}$: 1.3 fC. A tracking array consisting of three end-cap modules: 312, 310 and 308 *(top)*, three barrel modules: 0034, 007 and 0047 *(center)* and a four module barrel array, the three previous plus 0044 *(bottom)*.

Figures 12(a) and 12(b) show the correlation between the product of the plane efficiencies and the tracking efficiency. Each point represents a run, at a certain threshold and bias voltage.

The hypothesis is found to hold quite accurately. The slope of a fit through the points is close to 1 and the offset is compatible with 0. The maximum deviation of the points is less than 1 %.
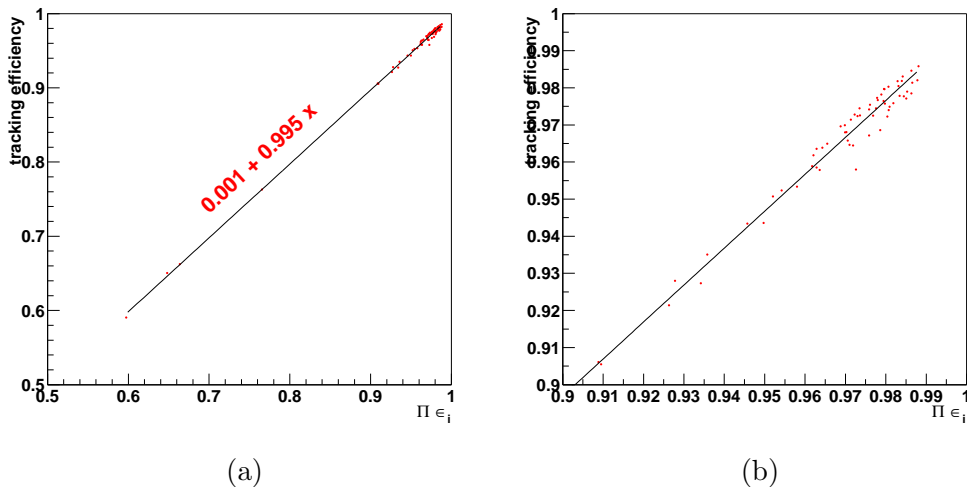
Fig. 12. Tracking efficiency versus the product of the plane efficiencies *(a)* and a detailed view of the highest efficiencies*(b)*

5 Helix fit - comparison with simulation

The beam in H8 consists of 180 GeV pions with a small mixture of high-momentum muons. In the absence of a magnetic field the tracks are straight. The linear fit in two dimensions has 4 free parameters. A helix fit (as used in ATLAS) has one more parameter that needs to be constrained. In this section, the effects of the extra degree of freedom on the results is discussed. The results are compared with a simulation and reconstruction of the SCT using ATLSIM [**?**] and ATRECON [11].

In this section the straight line fit of the previous analysis is replaced by a helix - a circle in the XZ plane and a straight line in the XY plane. Straight tracks are fit as a helix with a very small curvature: ie the measured momentum goes to infinity. But, this fit also allows for hits that do not form a straight line to form a track as long as the resulting momentum is higher than a certain cut-off. Depending on the value of this cut-off the fake rate can increase quite dramatically. Here, as in the TDR studies, a minimum transverse momentum of 2 GeV is required.

As expected, the helix fit leads to a deterioration of the performance with respect to the results obtained with straight tracks. Figure 13 shows the efficiency and fake rate versus discriminating threshold. The fake rate obtained for 97 % efficiency is ~ 1 % for a noise occupancy of $\sim 5 \cdot 10^{-3}$). Reducing the noise occupancy to $2 \cdot 10^{-3}$ by raising the threshold 0.1 fC leads to a reduction of the fake rate to $5 \cdot 10^{-4}$. A further 0.1 fC increase of the threshold yields a fake rate compatible with 0.
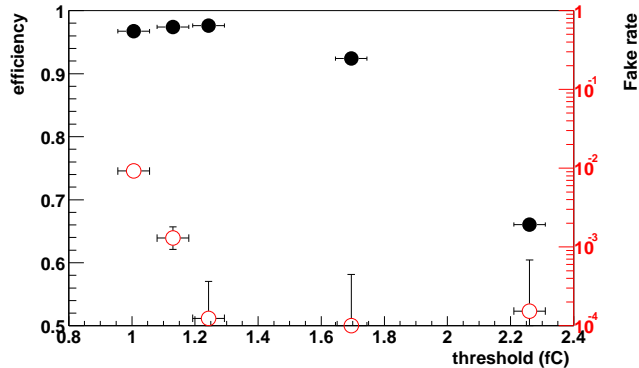
14

Fig. 13. Tracking efficiency and fake rate versus (corrected) discriminator threshold. Detector bias is 500 Volts on the HV supply, resulting in 470-490 Volts on the detector. A tracking array consisting of four barrel modules: 0034, 007,0047 and 0044

The track fit results can be used to estimate the track parameter resolutions. A virtual interaction point is simulated from the track reconstructed in the beam telescope. The distance of the interaction point to the first module is taken to be the radius of the first SCT barrel, 21 cm. The transverse and longitudinal impact parameters are the shortest distance in the $R\phi$ and Rz planes between the track and the interaction point. The corresponding measures in the test beam are the X and Y residual evaluated at the simulated interaction point. Similarly, the two angles of the ATLAS coordenate system ϕ and $\cot\theta$ at the point of closest approach to the interaction point are identified with the gradients dx/dz and dy/dz evaluated at the simulated interaction point.

The test beam results are compared to a simulation of the ATLAS detector in GEANT3 (ATLSIM). To evaluate the performance in similar circumstances, single pions/muons are generated in a small region around $\eta = 0$. The small (of the order of mradians) variation in incidence angles ϕ and θ are chosen in agreement with those observed in the test beam. In the simulation, the transverse momentum of the particles is chosen to be 500 GeV (to be compared with the *infinite* momentum in the beam test. The digitisation of the GEANT hits includes the simulation of noise hits. The simulated Equivalent Noise Charge of 1875 electrons is close to what is observed on the irradiated modules.

The simulated events are reconstructed using xKalman++ in the ATRE-CON [11] framework. The PIXEL and TRT data are not reconstructed, but the material of the detectors is in the simulation. The efficiency of the simulated stand-alone SCT for isolated muons is found to be 92 %, corresponding to a single-plane efficiency of 99 %. The fake rate is negligible in the absence of pile-up.

In figure 14 and 15 the residual distribution for the impact parameter and ϕ obtained in the beam test using the helix fit algorithm are compared to the

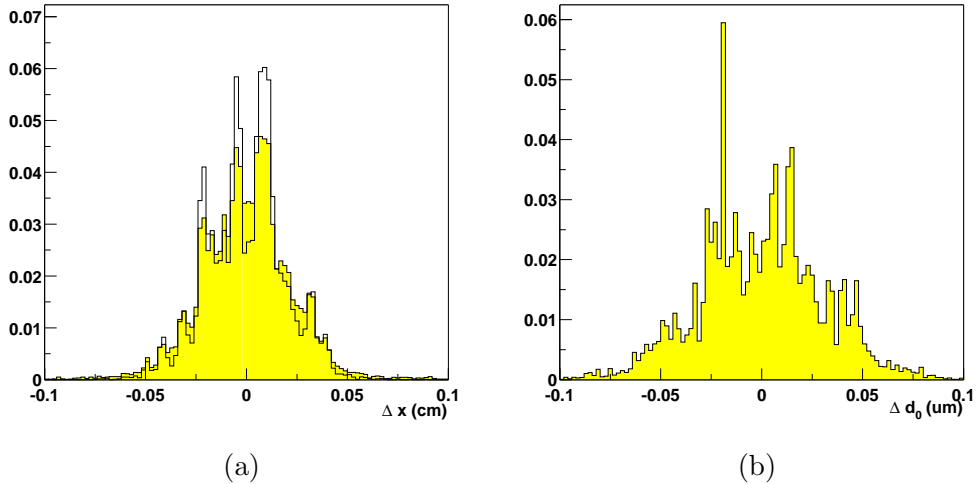simulation result for the stand-alone SCT.

(a)   (b)

Fig. 14. The transverse impact parameter distribution obtained from the test beam analysis: the filled histogram corresponds to 1.0 fC, the empty histogram to 1.2 fC ($V_{bias} = 500$ Volts) (a) and from a simulation of the SCT (b)
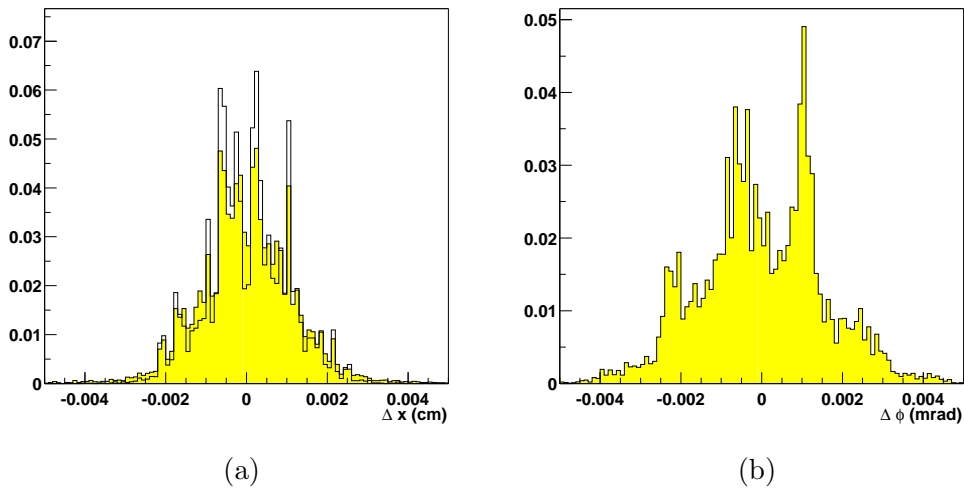

(a)   (b)

Fig. 15. The ϕ distribution obtained from the test beam analysis: the filled histogram corresponds to 1.0 fC, the empty histogram to 1.2 fC ($V_{bias} = 500$ Volts) (a) and from a simulation of the SCT (b)

Both the test beam result and the simulated distributions show significant non-Gaussian structures. As discussed before, these are a result of the discrete measurement of silicon strip detectors, especially important in binary readout systems. Inclusion of the pixel detectors in the helix fit and/or averaging over all $|\eta|$ and ϕ space smoothes out the distributions so that they become nearly Gaussian.

16

The results in figures **??** and **??** correspond to a discriminator threshold on all modules of 1.0 fC (fill colour) and 1.2 fC (the superposed empty histogram). For the lower threshold the noise occupancy becomes relevant and the probability that a track is *spoilt* by the addition of a noise hit is no longer negligible. This effect is reflected in the slightly broader distribution of the 1.0 fC run.

The resolution of the track parameters are taken to be the Root Mean Square of the distributions of figure 14 and 15 and similar distributions for the remaining parameters. The beam test results for two discriminator thresholds corresponding to a noise occupancy of $5 \cdot 10^{-3}$ and $5 \cdot 10^{-4}$ are listed in table **??**. In the same table the track parameter resolutions obtained from a simulation of the ATLAS precision tracker (SCT+pixels) and a stand-alone SCT are listed for comparison. The track resolutions from the beam test agree rather well with the expectation from the simulation.

		TB Tracking		Simulation	
		$1fC$	$1.2fC$	SCT	PT
$\sigma(1/p_T)$	(TeV^{-1})	3.8	3.6	6.0	0.8
$\sigma(\phi)$	(mrad)	1.1	1.0	1.5	0.1
$\sigma(cot\theta)$		0.0053	0.0041	0.0045	0.0007
$\sigma(d_0)$	(cm)	0.022	0.019	0.030	0.001
$\sigma(Z_0)$	(cm)	0.18	0.17	0.18	0.01

Table 1
The resolution of the helix parameter of reconstructed, isolated, high p_T tracks determined in the test beam tracking study and a simulation of the precision tracker (pixel+SCT) and standalone SCT

6   Perspective

In the Technical Design Report of the ATLAS Inner Detector [1], results for the tracking efficiency and fake of the full Inner Detector are given. Figures 16 form the essential result for the tracking performance.

Comparison of the simulations in the Technical Design Report and measurements in the test beam are not straight forward. Some quite substantial differences exist between both systems:

- In the beam test, all events contain a single straight and isolated track. Fake and spoiled tracks only arise from the different combinations of signal and noise hits. In the simulation of the full detector the signal occupancy is as high as 1 %. Tracks can be spoiled by interactions of the tracks inside the
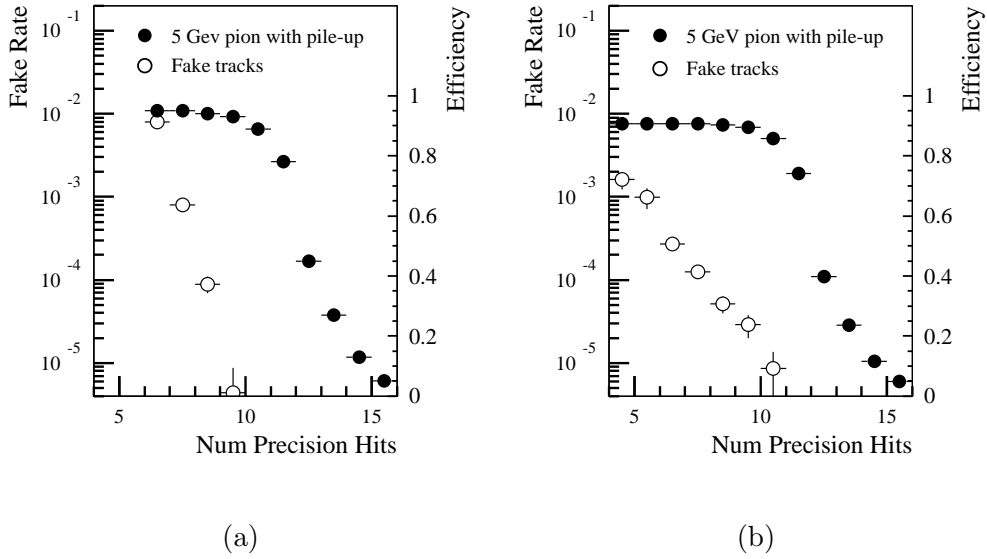
(a)   (b)

Fig. 16. The efficiency and fake rate for different requirements on the total number of Silicon hits on the track, obtained using the iPatRec algorithm *(a)* and the xKalman algorithm *(b)*. Taken from [1]

   detector.

- In all studies in the TDR, at least two PIXEL hits are required in the track reconstruction. Remember that PIXEL hits provide a three-dimensional space point measurement, whereas two SCT hits are needed to define a point in space.

The effects that these differences have on the efficiency and fake rate are hard to quantify. In this section, the test beam data are reanalysed in order to minimize the effect of the above points and thus render a result that is comparable to the TDR studies.

A high occupancy is obtained by overlaying various real events. For four overlaid events, the signal occupancy is of the order of 0.5 %. Note that all tracks fall in the 1 cm beam spot, ie locally the signal occupancy is much higher.

Finally, the track stub reconstructed in the PIXEL detector can be simulated by placing an XY point some distance along the track reconstructed by the analog telescope. The resolution can be made to coincide with that of the PIXEL detector by adding a random number from a uniform distribution with an appropiate width. Note that one point represents the three PIXEL layers.

The results from the test beam are shown in figure 17.

The first figure 17(a) shows the dependence of the tracking efficiency and fake rate on the number of Silicon hits required. The results correspond to an
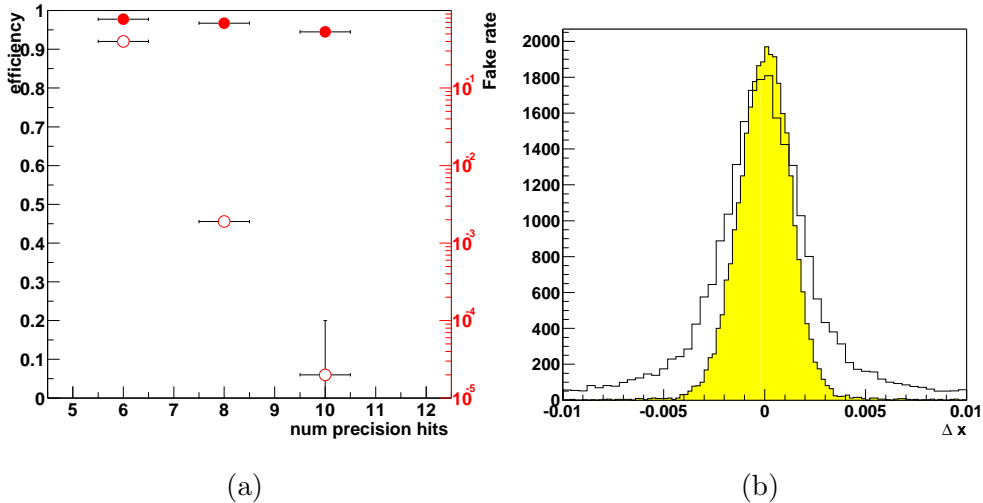
Fig. 17. The efficiency and fake rate obtained from the test beam data for different requirements on the tracks: the total number of Silicon hits *(a)* Error in the track parameter reconstruction *(b)* The filled histogram corresponds to a single-event analysis, whereas for the plain histogram four tracks from different events were superposed.

analysis of run 5668, at a bias voltage of 500 Volts and a noise occupancy of $\sim 5 \cdot 10^{-4}$, where 4 events were superposed. Thus, the signal occupancy is 0.5 % on the module. For the purpose of comparison TWO hits are counted for the pixel track stub [3]. The total number of hits is thus 2 + two times the number of SCT modules [4]. The efficiency loss is nearly constant up to 8 SCT hits (ie 10 precision tracker hits). The fake rate, on the other hand, falls very steeply with the number of hits required. This is in qualitative agreement with the prediction in 16(a).

The error of the intersect of the helix fit is slightly larger than that of the straight line fit due to the extra degree of freedom [5]. Moreover, when two tracks are very close, hits are sometimes assigned to the wrong track, leading to a distortion of the track parameters. These tracks are labelled spoiled. This effect is clearly visible as the tails in the track X intersect residual distributions in figure 17(b).

---

[3] In the TDR study two PIXEL hits are required.
[4] Due to the details of the tracking algorithm only even numbers of hits are used.
[5] The extra degree of freedom leads to a better fit in the sense that the line forms a better description of the points, ie the χ^2 is smaller. The error on the intersect, however, is larger

7 Conclusions

For the first time, tracks have been reconstructed through an array of irradiated SCT module prototypes. The efficiency with which tracks are found and the robustness against incorrect reconstructions - fake tracks - can be studied for a range of operating conditions. The most important parameter is the number of modules that make up the tracker. Scanning the discriminator threshold and detector bias voltage allow to study the effect of the efficiency and noise occupancy of the individual modules on the performance of the system.

For the three-module systems studied, the fake rate is reduced to well below 10^{-3} provided the noise occupancy of the individual planes is kept below or close to the ATLAS specification $(5 \cdot 10^{-4})$. The four-module array is quite robust against fake tracks: the fake rate is compatible with 0 for all thresholds that satisfy the noise occupancy specifation and increases only slightly for lower thresholds.

At the threshold needed to control the fake rate, the track reconstruction efficiencies of the three and four module arrays are over 97 %. The tracking efficiency is accurately predicted by the product of individual plane efficiencies.

Replacing the straight line fit with a helix, with an extra degree of freedom, leads to a slight deterioration of the results for the four-module array. At a noise occupancy close to the specified $5 \cdot 10^{-4}$ the fake rate is controlled to below 10^{-4}. The ATLAS GEANT3 simulation package has been used to simulate the response of the SCT to isolated MIPs. The results of the reconstruction using xKalman of the standalone SCT are compatible with the tracking results obtained in the beam test.

While the above results show the trends of tracking performance versus operating parameters, comparison with detailed simulations is not straight-forward. To bridge this gap, an attempt has been made to approximate the ATLAS environment as closely as possible. This includes a rough simulation of the track stub provided by the PIXEL detector, fitting the tracks with a helix and signal occupancies comparable to those expected from pile up events. On qualitative level, the dependence of the tracking performance on the number of Silicon hits and on the transverse momentum required agree with those predicted in the TDR.

Acknowledgements

References

[1]   the ATLAS Inner Detector Community, Inner Detector Technical Design Report volume I, ATLAS TDR 4, CERN/LHCC97-16

[2]   J.E. Garcia et al., Beamtests of ATLAS SCT Modules in 2002, ATLAS Internal Note in preparation.

[3]   A.Barr et al., Beamtests of ATLAS SCT Modules in August and October 2001, submitted as ATLAS internal note (ATL-COM-INDET-2002-017)

[4]   A.Barr et al., Results from an LHC structured beam test on SCT module prototypes, submitted as ATLAS Internal Note (ATL-COM-INDET-2002-018)

[5]   Y.Unno et al., Beam test of non-irradiated and irradiated ATLAS SCT microstrip modules at KEK, Proceedings of the IEEE Nuclear Science Symposium, San Diego, November 2001. Accepted for publication in Trans. Nucl. Sci.

[6]   T. Akimoto et al., Beam study of irradiated ATLAS-SCT prototypes, Proceedings of the 5th Florence conference, NIM A 485 (2002) 67-72

[7]   A. Barr et al., Beamtests of Prototype ATLAS SCT Modules at CERN H8 in June and August 2000, ATLAS Internal Note ATL-INDET-2002-005

[8]   J. Bernabeu et al., Results from the 1999 H8 beam tests of SCT prototypes, ATL-INDET-2000-004, NIM A 466 (2001) 397-405

[9]   ABCD3T project specification, v1.2

[10] S.J.M Peeters, Alignment of the ATLAS precision tracker using tracks ATL-COM-INDET-99-007

[11] Offline software group, DRAFT ATLAS ATRECON manual (Version 0.015), ATLAS internal note ATL-SOFT-94-015